Sensors & Actuators: B. Chemical 382 (2023) 133567

Contents lists available at ScienceDirect

Sensors and Actuators: B. Chemical

journal homepage: www.elsevier.com/locate/snb

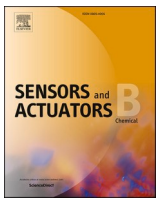

A niobium pentoxide waveguide sensor for on-chip mid-infrared absorption spectroscopic methane measurement

Ran Bi [a,1], Mingquan Pi [a,1], Chuantao Zheng [a,*], Huan Zhao [a], Lei Liang [b], Fang Song [a], Dingdi Wang [a,*], Yu Zhang [a], Yiding Wang [a,*], Frank K. Tittel [c]

[a] State Key Laboratory of Integrated Optoelectronics, College of Electronic Science and Engineering, Jilin University, Changchun 130012, China
[b] State Key Laboratory of Luminescence and Applications, Changchun Institute of Optics Fine Mechanics and Physics, Chinese Academy of Sciences, Changchun 130033, China
[c] Department of Electrical and Computer Engineering, Rice University, 6100 Main Street, Houston, TX 77005, USA

ARTICLE INFO

Keywords:
Gas sensor
Infrared absorption spectroscopy
Metal oxide waveguide
Wavelength modulation spectroscopy
Methane detection

ABSTRACT

The advantages of integrating infrared (IR) waveguide gas sensors on a chip include compactness, low power consumption, and high selectivity. Mid-IR waveguide sensors could be made of a variety of metal oxides with merits of low cost, high stability, transparency in the visible-IR spectrum, and non-toxicity. However, because most metal oxides have low refractive index, they are rarely used as waveguide core materials. To overcome this limitation, we chose niobium pentoxide (Nb_2O_5), a transparent material with high refractive index in the 0.35–10 μm wavelength range, as the core layer. We fabricated a Nb_2O_5 rectangular waveguide gas sensor using magnetron sputtering and lift-off process. The Nb_2O_5 waveguide with an external confinement factor of 11.5% was used for on-chip methane measurement at 3.291 μm based on wavelength modulation spectroscopy. A detection limit of 348 parts per million was achieved with an optimal averaging time of 61.2 s for a 2 cm long waveguide. The reported Nb_2O_5 waveguide gas sensor not only broadens the waveguide sensor core material family from silicon, chalcogenide (ChG) glass to metal oxides, but also provides detailed preparation and characterization methods for such kind of waveguide device.

1. Introduction

Infrared (IR) absorption spectroscopy is a powerful tool for identifying various gas components [1], which is realized by analyzing the IR absorption spectrum of gas analytes [2]. For traditional discrete gas sensor systems, multi-pass cell assemblies (such as White cells, Herriot cells) improve light-gas interaction by increasing the absorption path length [3–5]. However, such systems are typically bulky, energy intensive, and susceptible to environmental vibrations. To meet the demand for easy access to IR gas sensors, people continue to miniaturize IR gas sensors that can be integrated into smartphones, tablets, and wearable devices [1,6,7]. Integrating a photonic waveguide on a chip allows for compact and field deployable sensors [8].

Traditional materials for waveguide sensors include silicon (Si) [9,10], silicon nitride [11,12], and chalcogenide (ChG) glass [13,14]. Metal oxides, e.g. niobium pentoxide (Nb_2O_5), molybdenum trioxide (MoO_3) and tantalum pentoxide (Ta_2O_5), show the advantages of low cost, high stability, transparency in the visible-IR spectrum, and non-toxicity [15–17]. However, because most metal oxides have low refractive index, there has been little research into fabricating mid-IR waveguide sensors from them. To overcome this limitation, we will fabricate waveguide sensors out of Nb_2O_5, a transparent material with a high refractive index (n, ~ 2) and a low extinction coefficient (κ, < 0.1) in the 0.35 – 10 μm wavelength range [16,18]. More importantly, Nb_2O_5 waveguide is suitable for on-chip sensing of numerous gas analytes with molecular absorption fingerprints in this region.

Nb_2O_5 has received very little attention as waveguide material over the last forty years [19]. Recently, Yoshiki Hayama et al. demonstrated the feasibility of fabricating a Nb_2O_5 horizontal slot waveguide using modern nanofabrication techniques (e.g. sputtering, e-beam lithography) [20]. In this paper, we will demonstrate how to fabricate a simple rectangular Nb_2O_5 waveguide using only magnetron sputtering and lift-off process. Also, we will show how to use a Nb_2O_5 waveguide as a gas sensor, with sensor performance validated at 3.291 μm for

* Corresponding authors.
E-mail addresses: zhengchuantao@jlu.edu.cn (C. Zheng), wangdingdi@gmail.com (D. Wang), ydwang@jlu.edu.cn (Y. Wang).
[1] These two authors contribute equally to this work

https://doi.org/10.1016/j.snb.2023.133567
Received 6 December 2022; Received in revised form 19 February 2023; Accepted 21 February 2023
Available online 26 February 2023

measuring methane (CH_4) concentration. The primary novelties of this work are: (1) Nb_2O_5 films prepared by magnetron sputtering are transparent and homogeneous, with high refractive index (~2) in the mid-IR; (2) a Nb_2O_5 waveguide for gas sensing is designed using theoretical modeling; (3) the Nb_2O_5 waveguide is fabricated using magnetron sputtering and lift-off process; and (4) the sensing capability of the Nb_2O_5 waveguide sensor is validated for on-chip CH_4 concentration measurement using wavelength modulation spectroscopy (WMS).

2. Preparation and characterization of Nb_2O_5 films

2.1. Nb_2O_5 film preparation

We deposited Nb_2O_5 films at room temperature on fused quartz substrates (15 × 15 × 0.5 mm^3, cut-off wavelength: ~ 5 μm) and zinc selenide (ZnSe) substrates (15 × 15 × 1.5 mm^3, cut-off wavelength: ~ 22 μm) using radio frequency magnetron sputtering with a Nb_2O_5 ceramic target (diameter: 46 mm, thickness: 3 mm, purity: 99.99%). The bare substrate was cleaned with acetone, ethanol, and deionized water prior to sputtering. The deposition chamber's base pressure before sputtering was set to $< 8 \times 10^{-6}$ Torr. Table 1 lists the key parameters during magnetron sputtering.

2.2. Characterization of Nb_2O_5 films

The X-ray diffraction (XRD) patterns were captured using an X-ray diffractometer (TTR III, Rigaku Corporation, Japan) with a Bragg–Brentano parafocusing geometry and a Cu Kα source (1.54184 Å). The morphology of Nb_2O_5 films was photographed using a field emission scanning electron microscope (JSM-7500 F, JEOL Ltd., Japan). The film thickness was measured using a probe-type surface profiler (XP-2, Ambios Technology Inc., United States). The UV–visible–IR transmission spectroscopy was examined using a UV–visible spectrophotometer (TU-1810, Beijing Purkinje General Instrument Co., China). The IR transmission spectra were obtained using a Fourier transform IR spectrometer (Nicolet iS50, Thermo Fisher Scientific Inc., United States). The refractive index of the film was determined using a spectroscopic ellipsometer (IR-VASE Mark II, J.A. Woollam Company, United States).

2.3. Optical and structural properties of Nb_2O_5 films

XRD measurements were performed to investigate the crystal structure of the Nb_2O_5 film. Fig. 1(a) shows the XRD pattern of a deposited Nb_2O_5 film. The broad peak at ~20° is attributed to the fused quartz substrate. There are no obvious crystalline peaks, indicating that the as-deposited film is amorphous [16,21]. The UV–visible–near-IR and near-IR to mid-IR transmission spectra of the Nb_2O_5 film with a thickness of 350 nm are depicted in Fig. 1(b) and (c), respectively. The Nb_2O_5 film has a high average transmittance of 82.55% within 350–1100 nm (Fig. 1(b)), and a good transmittance, averaging 88.67% in the range of 1.35–4.7 μm (Fig. 1(c)). The dip at 2.94 μm is caused by impurity absorption from hydroxide (OH^-) ions in the fused quartz substrate. The morphology of a 350 nm thick Nb_2O_5 film is depicted in the scanning electron microscopy (SEM) image in the inset of Fig. 1(a). The film is uniform with few defects and no visible grain boundaries on the surface.

Table 1
Parameters maintained during the deposition of Nb_2O_5 films.

Deposition Parameters	Values
Base pressure	8×10^{-6} Torr
Sputtering pressure	1×10^{-2} Torr
Target to substrate distance	14 cm
Ar gas flow rate	20 sccm
Substrate temperature	Room temperature
Sputtering power	80 W

The SEM results are consistent with the amorphous nature revealed by the XRD results.

The thickness, n, and κ of the Nb_2O_5 film can be determined using ellipsometry. The fitted thickness of the Nb_2O_5 film is 310 nm, in reasonable agreement with the surface profiler's measurement of 350 nm. The wavelength dependence of n and κ is shown in Fig. 2(a). The CH_4 absorption lines in the 2–10 μm range are plotted as a reference based on the molecular spectroscopic database [22]. The Nb_2O_5 film has high n values (~ 2) and low κ values (< 0.1) in the mid-IR. For example, $n = 2.04$ and $\kappa = 0.046$ at 3.291 μm, and a strong CH_4 absorption line is located nearby. As a comparison with other alkane gases, the absorbance curves of CH_4, ethane, propane and butane are shown in Fig. 2(b) within 3.290 – 3.292 μm, at a concentration level of 50000 parts per million (ppm) and an optical path length of 15 cm. Propane and butane have almost no absorption, while ethane has some small absorption peaks overlapping with CH_4. But the ethane absorbance is 8 times smaller than CH_4. Moreover, in practical applications, e.g. atmosphere monitoring, the ethane concentration is 100 – 1000 times smaller than CH_4. So ethane with small concentration levels has almost no effect on CH_4 measurement. Even though at large ethane concentration levels, the cross interference between ethane and CH_4 can be solved using our proposed algorithm [23].

3. Mid-IR Nb_2O_5 waveguide sensor for CH_4 measurement

3.1. Nb_2O_5 waveguide design and optimization

We propose a rectangular waveguide with a core of Nb_2O_5 ($n = 2.04$) and a lower cladding of SiO_2 ($n = 1.41$). The upper cladding is the target gas ($n = \sim 1$). The operating wavelength is 3.291 μm. The electromagnetic field distribution was simulated using the COMSOL Multiphysics software. Fig. 3 shows the effective refractive index (n_{eff}) of the TM_0 and TM_1 modes as a function of the core layer thickness, with a core width held constant at 5.2 μm. The electric field distribution in TM_0 mode is depicted in the inset of Fig. 3.

The confinement factor (Γ) of the external evanescent field in the upper cladding is [24].

$$\Gamma = \frac{n_g}{\mathrm{Re}\{n_{cm}\}} \frac{\iint n_{\mathrm{cm}}\, \varepsilon |E|^2 \mathrm{d}x\mathrm{d}y}{\iint_{-\infty}^{\infty} \varepsilon |E|^2 \mathrm{d}x\mathrm{d}y} \tag{1}$$

where n_g is the group refractive index, n_{cm} is the cladding refractive index (~ 1 for CH_4), and E and ε are the electric field and dielectric constant, respectively. According to Fig. 3, the core layer thickness should be within 524 – 726 nm for single-mode operation. In this range, Γ increases as the core thickness gets larger. As a tradeoff between single-mode operation and high Γ, we chose 650 nm as the core thickness. The Γ derived by Eq. (1) is 11.53% for a 650 nm thick and 5.2 μm wide waveguide.

During CH_4 measurement, the evanescent field is absorbed by CH_4 at particular wavelengths, such as the fundamental absorption wavelength at 3.291 μm. As a result, the intensity drop of the waveguide output light is related to CH_4 concentration, expressed as [25].

$$I_{\mathrm{out}} = I_{\mathrm{in}} \exp(-\Gamma \alpha_{CH_4} cL - \alpha_{CH_4} L) \tag{2}$$

where I_{out} and I_{in} are the intensities of the input and output light, respectively, α_{CH4} and α_{int} are the absorption coefficient and waveguide loss, respectively, L is the length of the sensing region, and c is the CH_4 concentration.

In addition to the waveguide modeling results, we analyzed the optical response of a 650 nm-thick Nb_2O_5 core layer. We fabricated a genuine 650 nm thick Nb_2O_5 film on a ZnSe substrate to verify its IR transparency. In Fig. 1(d), the 650 nm thick Nb_2O_5 film on the ZnSe substrate has a high transmittance over 1.35 – 10 μm, which is comparable to the bare ZnSe substrate. The dips in transmittance at ~ 3 μm, ~

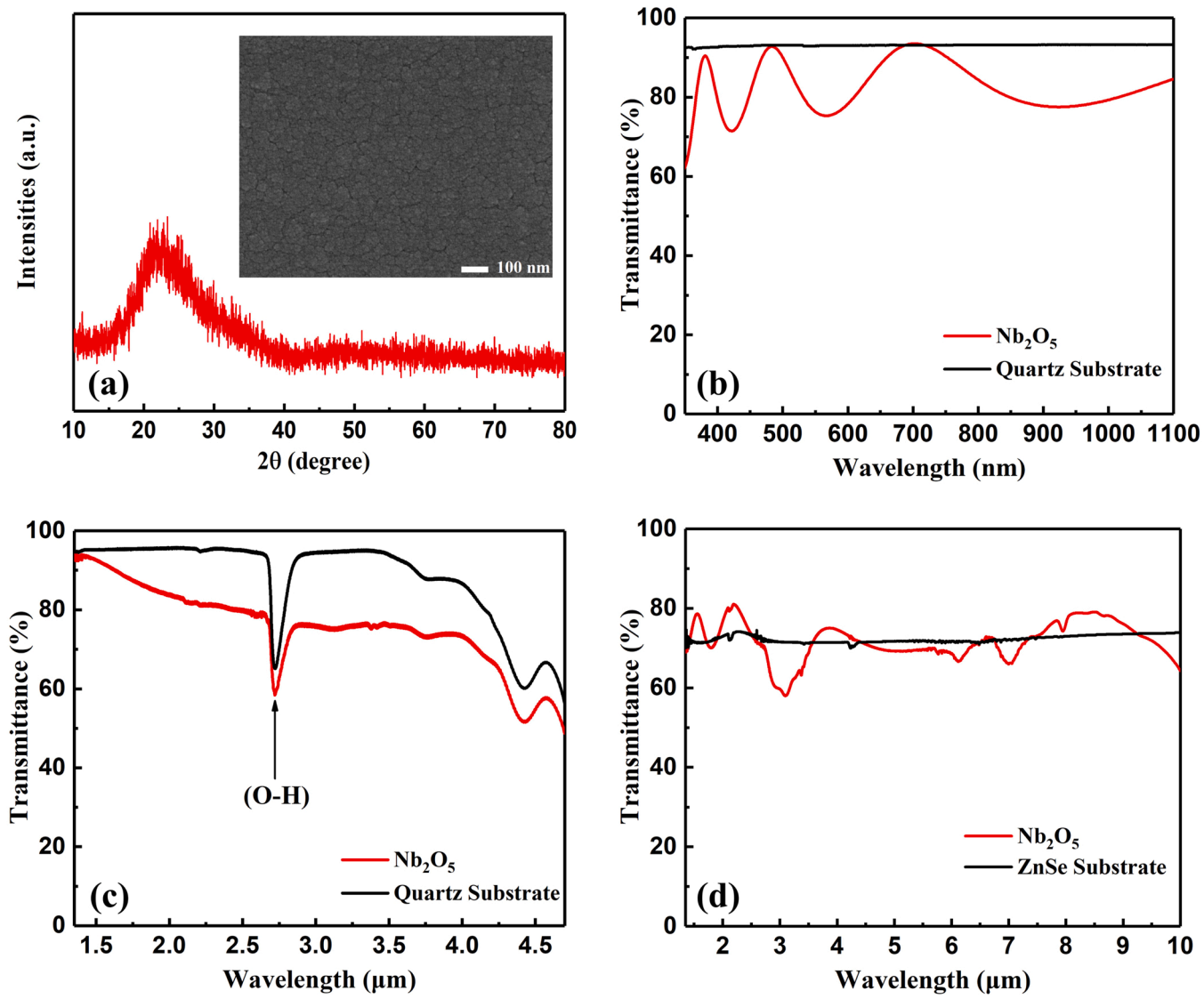

Fig. 1. Structure, morphology and optical properties of Nb_2O_5 films. (a) The XRD pattern of a 350 nm thick Nb_2O_5 film. The transmission spectra of a 350 nm thick Nb_2O_5 film deposited on a fused quartz substrate are shown in the (b) UV–visible–near-IR and (c) near-IR to mid-IR ranges, respectively. (d) The IR transmission spectrum of a 650 nm thick Nb_2O_5 film deposited on a zinc selenide substrate. The inset in (a) shows the SEM micrograph of a 350 nm thick Nb_2O_5 film deposited on a Si substrate.

6 μm and ~ 7 μm are most likely caused by absorption from niobium-oxygen bonds in the Nb_2O_5 film [26,27].

3.2. Fabrication of a Nb_2O_5 waveguide sensor

Fig. 4 depicts the magnetron sputtering and lift-off process to fabricate the Nb_2O_5 waveguide sensor. The waveguide was built on a Si substrate with a 2 μm thick SiO_2 layer. First, the substrate was spin-coated with the RN-218 photoresist to generate a 5 μm thick overcoat. The photoresist covering was photolithographically patterned and then developed to form a groove within it. The exposure dose was set to 60 mJ/cm^2 and the development duration to 180 s. After that, a 650 nm thick Nb_2O_5 film was deposited using magnetron sputtering. Finally, the photoresist was removed using acetone to reveal the Nb_2O_5 waveguide.

Fig. 5(a) depicts a schematic of the waveguide sensor, consisting of a sensing region in the center, two transition regions, and two coupling regions at both ends. The transition and coupling regions were used to improve fiber coupling efficiency. The coupling region has a width of 16 μm, which gradually decreases via the transition region (300 μm long) to 5.2 μm. Fig. 5(c) and (d) show the SEM micrographs of the coupling and sensing regions of the waveguide, respectively. Fig. 5(b) shows a SEM micrograph of the cross-section of the sensing region, which measures 5.2 μm in width and 650 nm in height, exactly matching the desired values. The length of the meandering sensing region is 2 cm, and the bend radius is 50 μm to reduce bend loss. The waveguide chip was bonded to a polydimethylsiloxane (PDMS) gas cell (16 mm × 10 mm ×10 mm inside), and the photograph in Fig. 6 shows how small this waveguide gas sensor is.

The waveguide loss was calculated using the cut-off method. The loss can be approximated using the formula $\alpha_{int} = -10 \log_{10} (Amp_{L2}/Amp_{L1})/ (L_2 - L_1)$, where L_1 and L_2 are the lengths of two different waveguides, and Amp_{L1} and Amp_{L2} correspond to the output light intensities for the two waveguides, respectively. We ran an experiment using two waveguides with lengths of 1 cm (straight) and 2 cm (meander), respectively. The gas chamber was filled with flowing nitrogen (N_2). The amplitudes of the two output signals were measured to be 729.8 mV and 482.1 mV, respectively. Then the waveguide loss was estimated to be $\alpha_{int} = 6.06$ dB/cm, primarily caused by the surface roughness or inherent defects in the as-deposited films.

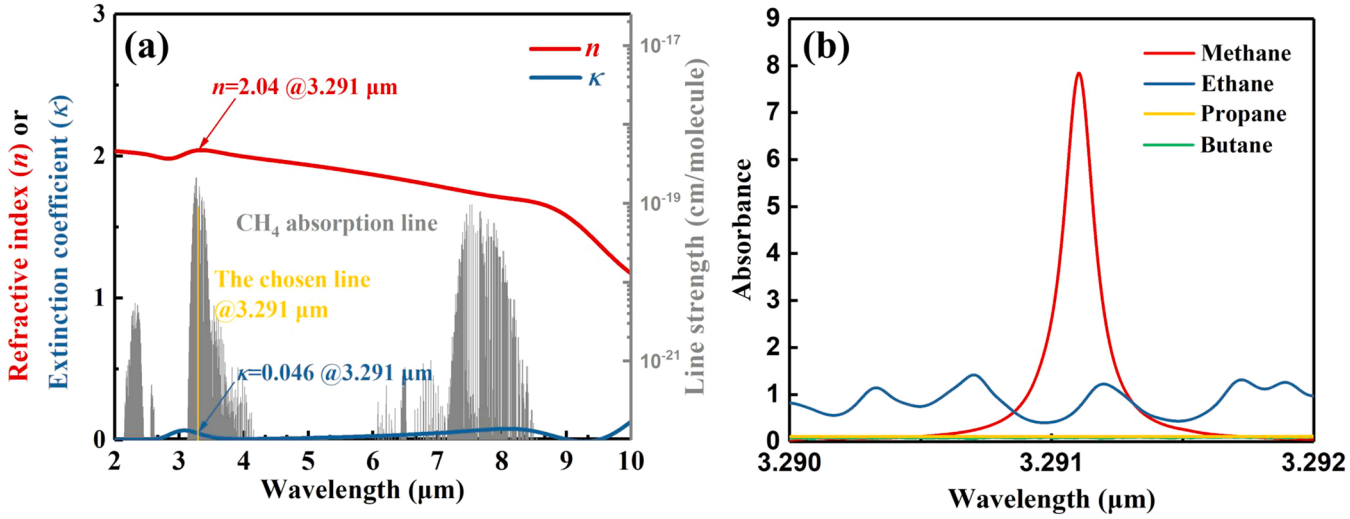

Fig. 2. (a) The refractive index (n) and extinction coefficient (κ) of the Nb_2O_5 film as a function of wavelength. The CH_4 absorption lines are plotted as a reference. (b) The absorbance curves of CH_4, ethane, propane and butane within 3.290–3.292 μm at a concentration level of 50000 ppm and an optical path length of 15 cm.

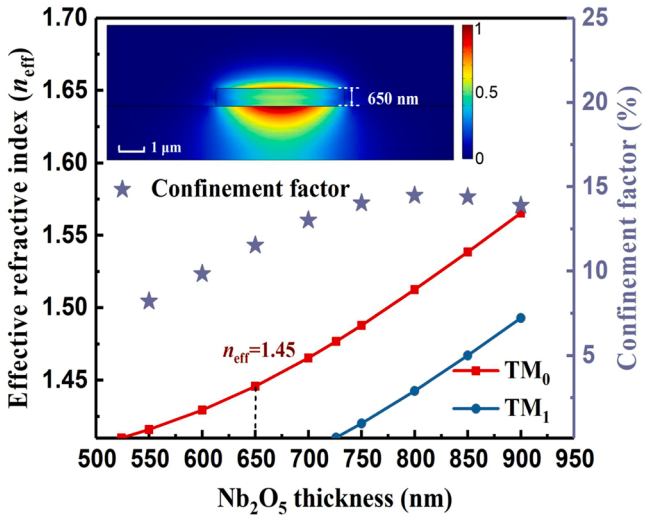

Fig. 3. The effective refractive index (n_{eff}) of the waveguide in TM_0 and TM_1 transmission modes, as well as the confinement factor of the single-mode (TM_0) waveguide, as a function of the core layer thickness. The core width is fixed at 5.2 μm. Inset: The electric field distribution in TM_0 mode of a 650 nm thick and 5.2 μm wide rectangular Nb_2O_5 waveguide.

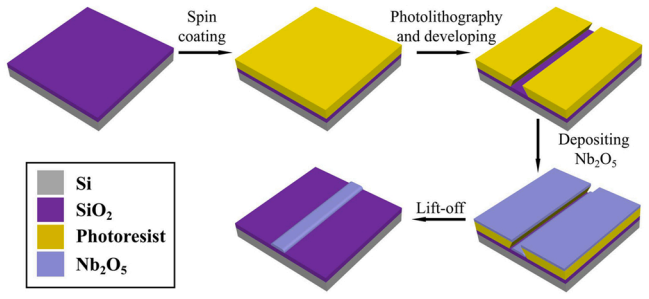

Fig. 4. The magnetron sputtering and lift-off process for fabricating the Nb_2O_5 waveguide.

3.3. CH_4 concentration measurement using a Nb_2O_5 waveguide sensor system

Fig. 6 depicts the block diagram of a mid-IR Nb_2O_5 waveguide gas sensor system. The light source was a 3.291 μm interband cascade laser (Nanoplus, Germany). The laser beam was coupled into a single-mode fluoride fiber (Le Verre Fluoré, France) via a reflective collimator (RC08, Thorlabs, Inc., United States). The output beam from the fiber was coupled into the waveguide. The output beam intensity was measured using a mercury cadmium telluride (MCT) detector (PVI-4TE-5, VIGO Photonics, Poland).

WMS was adopted for CH_4 measurement. Using high-frequency wavelength modulation (resulting in absorption coefficient modulation) and coherent demodulation, the $1/f$ noise can be suppressed for signal-to-noise ratio (SNR) enhancement. Compared to direct absorption spectroscopy (DAS), WMS can reduce the limit of detection (LoD) by a factor of 5 – 10. The sine-wave modulation frequency and the triangular-wave scan frequency are typically in the order of kHz and Hz, respectively. These two frequencies are decided by the parameters of the laser driver electronics, and determine the integral time of the digital lock-in amplifier. In this work, the two frequencies were set to 5 kHz and 10 Hz, respectively, resulting in an acceptable data sampling rate by hardware and enough data for high-resolution spectrum processing. The 10 Hz triangular-wave signal was used to periodically tune the laser wavelength across the 3.291 μm absorption line. The 5 kHz sine-wave signal was used to modulate the laser wavelength so as to extract the sine modulation wave's second harmonic ($2f = 10$ kHz) signal through the lock-in amplifier. The maximum amplitude of the $2f$ signal ($\max(A_{2f})$), proportional to CH_4 concentration, was used for concentration determination with a high accuracy.

The amplitude of the sine-wave signal represents modulation depth (i.e. the amplitude of the modulated laser wavenumber), which determines the $2f$ signal amplitude and needs to be optimized. Fig. 7 shows the variation curve of $\max(A_{2f})$ as a function of the sine-wave amplitude at a concentration level of 3×10^5 ppm. The highest $\max(A_{2f})$ is obtained when the modulation amplitude is 0.03 V, and the optimal modulation depth is 0.09 cm^{-1}.

In sensor calibration, a 100 standard cubic centimeters per minute (sccm) CH_4 in N_2 flow was directed through the gas cell. A gas mixing system (Series 4000, Environics, United States) controlled the CH_4 concentration. Fig. 8(a) shows the measured $2f$ signal waveforms for the 10^5–10^6 ppm CH_4 in N_2. In Fig. 8(b), curve of $\max(A_{2f})$ (in V) is plotted against CH_4 concentration (c, in ppm). The measurement data set was

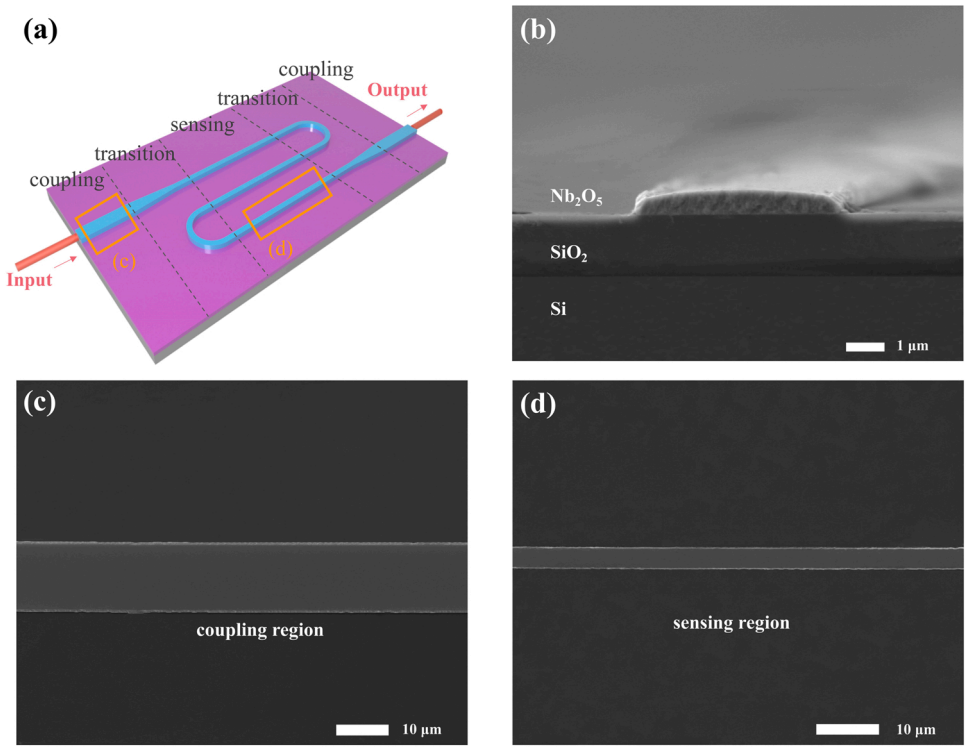

Fig. 5. (a) A schematic of the Nb_2O_5 waveguide sensor consisting of a sensing region, two transition regions and two coupling regions. (b) A SEM micrograph of the cross-section of the sensing region. (c, d) SEM micrographs of the (c) coupling region and (d) sensing region of the Nb_2O_5 waveguide.

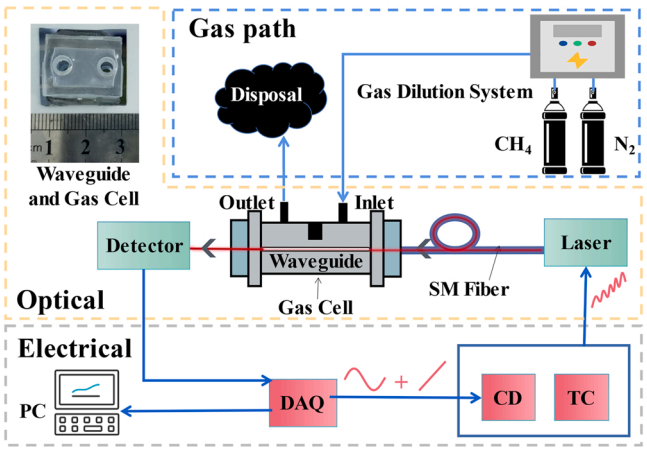

Fig. 6. The block diagram of a mid-IR Nb_2O_5 waveguide sensor system. CD: current driver, TC: temperature controller, SM: single mode, PC: personal computer, DAQ: data acquisition. In the upper left corner, a photograph of the PDMS gas cell bonded to the waveguide sensor is presented.

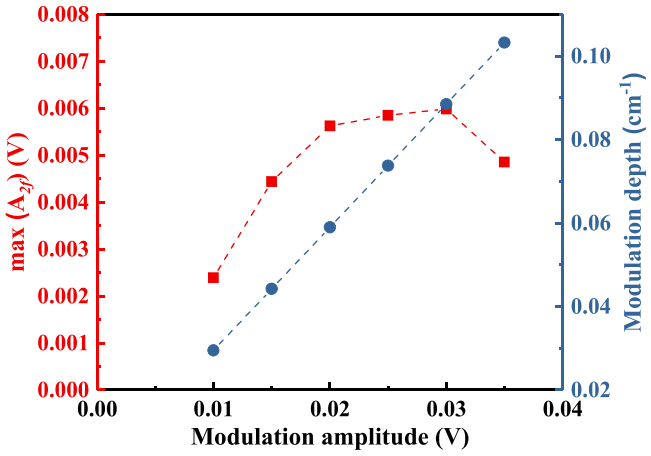

Fig. 7

Fig. 7. The 2*f* signal amplitude (max(A_{2f})) and modulation depth as a function of the sine-wave amplitude when the CH_4 concentration is 30%.

fitted by a straight line with the equation of

$$\max(A_{2f}) = 1.16 \times 10^{-8} \times c + 0.26 \times 10^{-2} \quad (3)$$

The good linear fit demonstrates a wide CH_4 measurement range from nearly 0–10^6 ppm for the sensor.

LoD is the lowest concentration (C_{min}) that can be detected by the sensor, mainly dependent on noise level. The standard or Allan deviation, is commonly used to calculate the LoD. For the Allan deviation analysis, the gas cell should be fed with pure N_2 flow. Fig. 9(a) depicts the reading of CH_4 concentration from the waveguide sensor as a function of measurement time. The data sampling period was 0.2 s, i.e. 0.1 s scan time plus 0.1 s data processing time, leading to a 2*f* signal acquisition rate of 5 Hz and 2000 data dots in total. The negative reading results from the inapplicability of Eq. (3) to a CH_4 concentration less than the LoD. Fig. 9(b) shows the Allan deviation as a function of averaging time (τ). The Gaussian white noise is suppressed as τ increases, lowering the Allan deviation. However, when τ exceeds a certain threshold, the Allan deviation begins to rise due to the gradual increase in system drift. The relation curve of LoD (ppm) versus τ (s) can be fitted by Eq. (4).

$$\text{LoD} = 2{\cdot}22\times10^4\exp(-5\tau) + 3{\cdot}41\times10^3\exp(-0{\cdot}25\tau) + 8{\cdot}23\times10^2,\ 0 \le \tau \le 400 \quad (4)$$

The LoD of the sensor can be characterized by the smallest Allan deviation, i.e. 348.6 ppm with τ = 61.2 s. In this case, the measurement

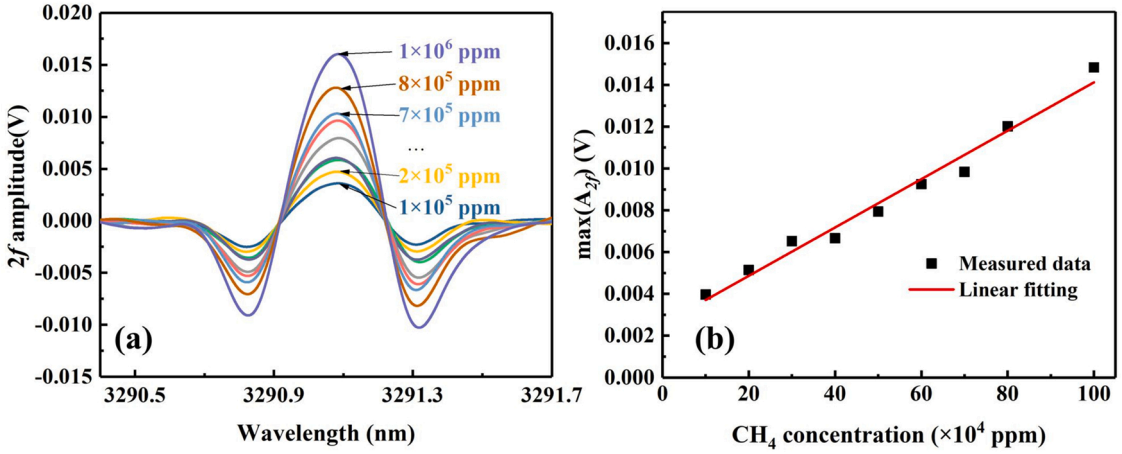

Fig. 8. (a) The measured 2*f* signal waveforms for 10^5–10^6 ppm CH_4 in N_2. (b) The measured data dots and linear fitting curve of max(A_{2f}) versus CH_4 concentration within the 10^5–10^6 ppm range.

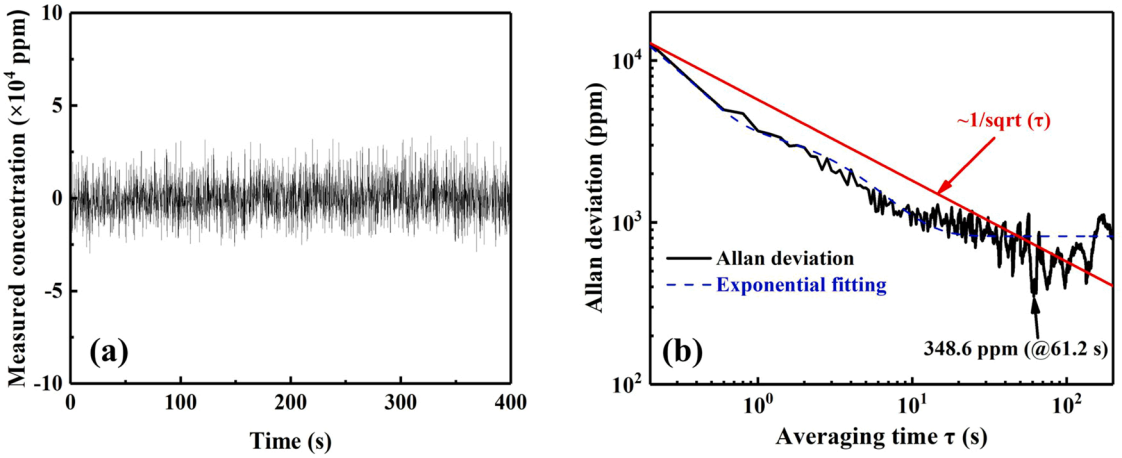

Fig. 9. (a) The CH_4 concentration measured by the Nb_2O_5 waveguide sensor in a pure N_2 environment as a function of measurement time. (b) The Allan deviation and fitting curve of the waveguide sensor versus averaging time. The red line ($\sim 1/\sqrt{\tau}$) indicates the Allan deviation of a Gaussian white noise dominated sensor.

range is 384 – 10^6 ppm. The LoD increases rapidly as τ decreases. When $\tau = 0.2$ s, the LoD reaches $\sim 1.28 \times 10^4$ ppm, corresponding to a measurement range of 1.28×10^4 – 10^6 ppm. In practical application, smoothing filtering can be used for data averaging, in order to suppress Gaussian white noise and improve measurement accuracy.

Resolution is the minimum concentration change ($\pm \Delta C$) that can be distinguished from the background concentration (C) by the sensor. Resolution is also related to noise level and will change with concentration for nonlinear systems. However, for our linear waveguide sensor (Fig. 8(b)), the resolution does not change with concentration and is therefore equal to the LoD.

During CH_4 measurement, the 2*f* signal amplitude may change because of light intensity variation caused by vibration for instance. To minimize the effect of light intensity change, in addition to maintaining the measurement setup stable, the background signal (representing light intensity) can be obtained by fitting the absorption signal output from the detector, followed by a ratio operation between the two signals before 2*f* signal extraction [28].

3.4. In comparison to waveguides made of other materials

Table 2 contrasts the Nb_2O_5 waveguide sensor with our reported ChG [24] and SOI [29] waveguide sensors. These sensors have the same sensing length of 2 cm, the same operating wavelength of 3.291 μm, and a similar structure. The advantages of the Nb_2O_5 waveguide sensor include low cost, simple preparation, high stability, transparency in the visible spectrum, and non-toxicity, which pave the way for mass production and commercialization of Nb_2O_5 sensors on a large scale. The only disadvantage of this sensor is its high waveguide loss (α_{int} = 6.06 dB/cm), and we are working on several methods to improve Nb_2O_5 quality in order to reduce waveguide loss.

Table 2
Comparison of the 2 cm long mid-IR waveguide CH_4 sensors.

	Key features	Nb_2O_5	SOI[29]	ChG[24]
Material properties	*n*	~2	~3.4	~2.6
	Transparent range	0.35–10 μm	2–8 μm	~1–20 μm
	Preparation process	Lift-off	Dry etching	Lift-off
	Toxicity	Low	Low	High
	Stability	High	High	Low
	Price (USD)	10	20	10
Waveguide sensor	Confinement factor	11.53%	34.3%	7.8%
	LoD	349 ppm (@ 306 s)	604 ppm (@ 0.2 s)	141 ppm (@ 32 s)
	α_{int}	6.06 dB/cm	0.71 dB/cm	1.52 dB/cm

4. Conclusions

In conclusion, instead of the traditionally reported silicon and ChG waveguide gas sensors, we demonstrated a novel Nb_2O_5 waveguide gas sensor based on IR absorption spectroscopy. Magnetron sputtering and lift-off process were used to fabricate the sensor. Nb_2O_5 has a wide transparency range of 0.35–10 μm, suitable for on-chip sensing of a variety of gases with molecular absorption fingerprints in this region. We measured CH_4 concentration using WMS at 3.291 μm. The Nb_2O_5 sensor has a LoD of 348 ppm and a maximum detectable concentration of 10^6 ppm. The reported Nb_2O_5 waveguide sensor broadens the waveguide core material family to include metal oxides, which is beneficial to mass production and commercialization of such waveguide sensors on a large scale.

CRediT authorship contribution statement

Ran Bi: Conceptualization, Methodology, Software, Writing – original draft. **Mingquan Pi**: Conceptualization, Methodology, Software, Validation. **Chuantao Zheng**: Conceptualization, Methodology, Supervision, Writing – review & editing. **Huan Zhao**: Hardware circuit. **Lei Liang**: Methodology, Validation. **Fang Song**: Writing– original draft preparation. **Dingdi Wang**: Conceptualization, Methodology, Writing – review & editing. **Yu Zhang**: Supervision. **Yiding Wang**: Writing – review & editing, Supervision. **Frank. K. Tittel**: Writing – review & editing.

Declaration of Competing Interest

The authors declare that they have no known competing financial interests or personal relationships that could have appeared to influence the work reported in this paper.

Data Availability

Data will be made available on request.

Acknowledgements

The authors would like to express their gratitude to the National Natural Science Foundation of China (Nos. 62175087, 62235016, 62105118, 61960206004), Key Science and Technology Research and Development Program of Jilin Province, China (No. 20200401059GX), and the Key Research and Development of Changchun (No. 21ZGN24).

References

[1] D.M. Kita, H. Lin, A. Agarwal, K. Richardson, I. Luzinov, T. Gu, J. Hu, On-chip infrared spectroscopic sensing: redefining the benefits of scaling, IEEE J. Sel. Top. 23 (2017) 340–349.
[2] J. Hodgkinson, R.P. Tatam, Optical gas sensing: a review, Meas. Sci. Technol. 24 (2013), 012004.
[3] J. Glockler, C. Jaeschke, Y. Kocaoz, V. Kokoric, E. Tutuncu, J. Mitrovics, B. Mizaikoff, iHWG-MOX: a hybrid breath analysis system via the combination of substrate-integrated hollow waveguide infrared spectroscopy with metal oxide gas sensors, ACS Sens 5 (2020) 1033–1039.
[4] V. Kokoric, A. Wilk, B. Mizaikoff, iPRECON: an integrated preconcentrator for the enrichment of volatile organics in exhaled breath, Anal. Methods 7 (2015) 3664–3667.
[5] P.R. Fortes, J.F. da Silveira Petruci, A. Wilk, A.A. Cardoso, I.M. Raimundo Jr, B. Mizaikoff, Optimized design of substrate-integrated hollow waveguides for mid-infrared gas analyzers, J. Opt. 16 (2014), 094006.
[6] D. Popa, F. Udrea, Towards integrated mid-infrared gas, Sensors, Sensors 19 (2019) 2076.
[7] R. Bogue, Recent developments in MEMS sensors: a review of applications, markets and technologies, Sens. Rev. 33 (2013) 300–304.
[8] P. Nizamidin, A. Yimit, J. De Wang, K. Itoh, Optical properties and sensing applications of lithium iron phosphate thin films, Thin Solid Films 520 (2012) 6250–6255.
[9] T. Hu, B. Dong, X. Luo, T.-Y. Liow, J. Song, C. Lee, G.-Q. Lo, Silicon photonic platforms for mid-infrared applications, Photon. Res. 5 (2017) 417–430.
[10] L. Tombez, E.J. Zhang, J.S. Orcutt, S. Kamlapurkar, W.M.J. Green, Methane absorption spectroscopy on a silicon photonic chip, Optica 4 (2017) 1322–1325.
[11] P. Tai Lin, V. Singh, L. Kimerling, A. Murthy Agarwal, Planar silicon nitride mid-infrared devices, Appl. Phys. Lett. 102 (2013), 251121.
[12] C. Ranacher, C. Consani, A. Tortschanoff, R. Jannesari, M. Bergmeister, T. Grille, B. Jakoby, Mid-infrared absorption gas sensing using a silicon strip waveguide, Sens. Actuator A Phys. 277 (2018) 117–123.
[13] A. Gutierrez-Arroyo, E. Baudet, L. Bodiou, J. Lemaitre, I. Hardy, F. Faijan, B. Bureau, V. Nazabal, J. Charrier, Optical characterization at 7.7 μm of an integrated platform based on chalcogenide waveguides for sensing applications in the mid-infrared, Opt. Express 24 (2016) 23109–23117.
[14] Z. Han, P. Lin, V. Singh, L. Kimerling, J. Hu, K. Richardson, A. Agarwal, D.T.H. Tan, On-chip mid-infrared gas detection using chalcogenide glass waveguide, Appl. Phys. Lett. 108 (2016), 141106.
[15] W. Park, G. Lee, J. Kim, Reactive-sputtered transparent MoO_3 film for high-performing infrared Si photoelectric devices, Sens. Actuator A Phys. 271 (2018) 251–256.
[16] Ö.D. Coşkun, S. Demirel, G. Atak, The effects of heat treatment on optical, structural, electrochromic and bonding properties of Nb_2O_5, thin films, J. Alloy Compd. 648 (2015) 994–1004.
[17] S. Sathasivam, B.A.D. Williamson, A. Kafizas, S.A. Althabaiti, A.Y. Obaid, S. N. Basahel, D.O. Scanlon, C.J. Carmalt, I.P. Parkin, Computational and Experimental Study of Ta_2O_5 Thin Films, J. Phys. Chem. C. 121 (2017) 202–210.
[18] F. Lai, L. Lin, Z. Huang, R. Gai, Y. Qu, Effect of thickness on the structure, morphology and optical properties of sputter deposited Nb_2O_5 films, Appl. Surf. Sci. 253 (2006) 1801–1805.
[19] S. Forouhar, R.X. Lu, W.S. Chang, R.L. Davis, S.K. Yao, Chirped grating lenses on Nb_2O_5 transition waveguides, Appl. Opt. 22 (1983) 3128.
[20] Yoshiki Hayama, Shinta Uchibori, Katsumi Nakatsuhara, Masayuki Takeda, Takeshi Nishizawa, Fabrication of Nb_2O_5 horizontal slot waveguide structures, 24th OECC and 2019 International Conference on PSC (2019) 1–3.
[21] A.A. Atta, A.M. Hassanien, M.M. El-Nahass, A.A. Shaltout, Y.A. Al-Talhi, A. M. Aljoudi, Influence of argon flow rate on structural and optical properties of transparent Nb_2O_5 thin films, Opt. Quantum Electron. 51 (2019) 341.
[22] I.E. Gordon, L.S. Rothman, R.J. Hargreaves, R. Hashemi, E.V. Karlovets, F. M. Skinner, E.K. Conway, C. Hill, R.V. Kochanov, Y. Tan, P. Wcisło, A.A. Finenko, K. Nelson, P.F. Bernath, M. Birk, V. Boudon, A. Campargue, K.V. Chance, A. Coustenis, B.J. Drouin, J.M. Flaud, R.R. Gamache, J.T. Hodges, D. Jacquemart, E.J. Mlawer, A.V. Nikitin, V.I. Perevalov, M. Rotger, J. Tennyson, G.C. Toon, H. Tran, V.G. Tyuterev, E.M. Adkins, A. Baker, A. Barbe, E. Canè, A.G. Császár, A. Dudaryonok, O. Egorov, A.J. Fleisher, H. Fleurbaey, A. Foltynowicz, T. Furtenbacher, J.J. Harrison, J.M. Hartmann, V.M. Horneman, X. Huang, T. Karman, J. Karns, S. Kassi, I. Kleiner, V. Kofman, F. Kwabia–Tchana, N. N. Lavrentieva, T.J. Lee, D.A. Long, A.A. Lukashevskaya, O.M. Lyulin, V. Y. Makhnev, W. Matt, S.T. Massie, M. Melosso, S.N. Mikhailenko, D. Mondelain, H. S.P. Müller, O.V. Naumenko, A. Perrin, O.L. Polyansky, E. Raddaoui, P.L. Raston, Z. D. Reed, M. Rey, C. Richard, R. Tóbiás, I. Sadiek, D.W. Schwenke, E. Starikova, K. Sung, F. Tamassia, S.A. Tashkun, J. Vander Auwera, I.A. Vasilenko, A.A. Vigasin, G.L. Villanueva, B. Vispoel, G. Wagner, A. Yachmenev, S.N. Yurchenko, The HITRAN2020 molecular spectroscopic database, J. Quant. Spectrosc. RA 277 (2022), 107949.
[23] D. Yu, F. Song, C. Zheng, L. Hu, Y. Ma, K. Zheng, Y. Zhang, Y. Wang, F.K. Tittel, Simultaneous CH4/CO measurement at atmospheric pressure using a single 2.3μm laser and a dual-gas cross-interference cancellation algorithm, IEEE T. Instrum. Meas. 71 (2022) 9503009.
[24] M. Pi, Y. Huang, H. Zhao, Z. Peng, J. Lang, J. Ji, L. Teng, F. Song, L. Liang, Y. Zhang, C. Zheng, Y. Wang, F.K. Tittel, Theoretical and experimental investigation of on-chip mid-infrared chalcogenide waveguide CH_4 sensor based on wavelength modulation spectroscopy, Sens. Actuators B Chem. 362 (2022), 131782.
[25] J. Charrier, M.-L. Brandily, H. Lhermite, K. Michel, B. Bureau, F. Verger, V. Nazabal, Evanescent wave optical micro-sensor based on chalcogenide glass, Sens. Actuators B Chem. 173 (2012) 468–476.
[26] C.C.M. Pereira, E.R. Lachter, Alkylation of toluene and anisole with 1-octen-3-ol over niobium catalysts, Appl. Catal. A: -Gen. 266 (2004) 67–72.
[27] L.J. Burcham, J. Datka, I.E. Wachs, In situ vibrational spectroscopy studies of supported niobium oxide catalysts, J. Phys. Chem. B 111 (1999) 6015–6024.
[28] W. Ye, C. Li, C. Zheng, N.P. Sanchez, A.K. Gluszek, A.J. Hudzikowski, L. Dong, R. J. Griffin, F.K. Tittel, Mid-infrared dual-gas sensor for simultaneous detection of methane and ethane using a single continuous-wave interband cascade laser, Opt. Express 24 (2016) 16973–16985.
[29] H. Zhao, C. Zheng, M. Pi, L. Liang, F. Song, Y. Zhang, Y. Wang, F.K. Tittel, On-chip mid-infrared silicon-on-insulator waveguide methane sensor using two measurement schemes at 3.291 μm, Front. Chem. 10 (2022), 953684.

Ran Bi earned her bachelor's degree in 2018 from Jilin University's College of Electronic Science and Engineering in China. She began her PhD studies in 2020. She now majors in Circuit and System, and her research interests include infrared transparent conductive films and their applications.

Mingquan Pi earned his bachelor's degree in 2018 from Jilin University's College of Electronic Science and Engineering in China. He began his PhD studies in 2020. He now majors in Circuit and System, and his research interests include waveguide gas sensor and optical waveguide device.

Chuantao Zheng earned his master's degree and PhD from Jilin University's College of Electronic Science and Engineering in 2007 and 2010, respectively. He is currently a professor at Jilin University in China. His research interests include optoelectronic devices and their applications in optical sensing. Prof. Zheng has contributed as a first or corresponding author to over 180 scientific journal articles in the aforementioned technical fields.

Huan Zhao earned his bachelor's degree in 2017 from Jilin University's College of Electronic Science and Engineering in China. He began his PhD studies in 2019. He now majors in Circuit and System, and his research interests include hybrid integrated laser and optical waveguide device.

Lei Liang earned his PhD from the College of Electronic Science and Engineering at Jilin University in 2014. He is currently an associate researcher at the State Key Laboratory of Luminescence and Applications, Changchun Institute of Optics Fine Mechanics and Physics, Chinese Academy of Sciences. His research interests include optical waveguide device, semiconductor lasers, and semiconductor optical amplifiers.

Fang Song earned her bachelor's degree in 2011 from Changchun University of Science and Technology's College of Electronic and Information Engineering. She earned her master's degree and PhD from Jilin University's College of Electronic Science and Engineering in 2014 and 2020, respectively. She is currently a lecturer at Jilin University in China. Her research interests include gas and bio-medical sensing techniques and applications.

Dingdi Wang earned his bachelor's degree from Nanjing University in 2009 and his PhD from Hong Kong University of Science and Technology in 2013. He is now a postdoctoral fellow at Jilin University. His research interests include transparent conductive films and carbon structures.

Yu Zhang earned his master's degree and PhD from Jilin University's College of Electronic Science and Engineering in 2007 and 2010, respectively. He is now a professor at the same university. His research interests include quantum dot materials, LEDs, and solar cells.

Yiding Wang earned his master's degree in Physics from Jilin University in 1991. He is currently a professor at Jilin University's College of Electronic Science and Engineering. He is involved in the fields of infrared gas sensors and the fabrication of mid-infrared LEDs and LDs.

Frank K. Tittel earned his bachelor's degree in 1955 and PhD in 1959 from Oxford University. He is now the J. S. Abercrombie Professor in Rice University's Electrical and Computer Engineering Department. Prof. Frank Tittel has been involved in many innovative developments in quantum electronics and laser technology since the invention of the laser in 1960, with applications ranging from laser spectroscopy to environmental monitoring. The most recent designs utilize quantum cascade and interband cascade lasers to achieve compact, robust instrumentation that can be deployed for field applications, such as at NASA's Johnson Space Center related for air and water quality issues relevant to the International Space Station, for urban formaldehyde monitoring funded by the Environmental Protection Agency, and for non-invasive NO and CO detection in biomedical systems funded by the National Institute of Health (http://lasersci.rice.edu/).